Korean J. Chem. Eng., **30**(11), 2026-2029 (2013)
DOI: 10.1007/s11814-013-0133-5

Effects of dye etching on the morphology and performance of ZnO nanorod dye-sensitized solar cells

Jiyuan Yang, Yu Lin†, and Yongming Meng

College of Material Science and Engineering,
Engineering Research Center of Environment-Friendly Functional Materials for Ministry of Education,
Huaqiao University, Xiamen, Fujian 361021, P. R. China
(*Received 5 May 2013 • accepted 24 July 2013*)

Abstract−Dye-sensitized solar cells based on electrodeposited ZnO nanorod arrays were fabricated and tested. Field-emission scanning electron microscopy (FESEM) and X-ray powder diffraction (XRD) were used to identify the characters of ZnO nanorod arrays. The effects of dye etching on the morphology and performance of ZnO nanorod dye-sensitized solar cells were studied. It was found that the surfaces of ZnO nanorods were both etched by dye solutions, no matter N3 or N719. Compared with N3, N719 had a larger damage to the structure of ZnO nanorod photoanode, and the photoelectric conversion efficiency of cells decreased quickly with the sensitizing time increasing. In a certain range, the increasing length of ZnO nanorods can clearly improve the photoelectric conversion efficiency of cells.

Key words: Dye Etching Zinc Oxide Nanorod, Morphology, Cell Performance, Dye-sensitized Solar Cells

INTRODUCTION

Dye-sensitized solar cell (DSSC), a neoteric power conversion device, has attracted substantial attention since its first appearance in 1991 due to its low cost, simple fabrication and enormous application prospect [1]. Typical DSSCs are a sandwich structure that consists of three parts: a dye-sensitized metal-oxides layer as working electrode, an electrolyte containing a redox couple (I^-/I^{3-}) and a counter electrode with a Pt layer. Much concern has been focused on the photoanode, which is the pivotal component of DSSCs that plays a significant role for charge collection and transmission. Up to now, the best performance reported in the literature has been obtained with cells composed of a titania (TiO_2) nanoparticulate thin film [2-5].

Besides TiO_2, zinc oxide (ZnO) is also investigated as another promising candidate for anode materials [6-10]. The band gap energy and conduction band edge of ZnO are similar to those of TiO_2 [11, 12]. Additionally, ZnO showed an order of magnitude higher electron mobility and the corresponding electron diffusion coefficient [13]. Especially, vertically grown ZnO nanorods have been used in DSSCs with an understanding that the use of single crystal nanorods may allow electron transport via extended sites in the conduction band, rather than a series of hoppings between the traps [14-16]. Recently, DSSCs based on ZnO nanorod arrays, produced by CVD [17] and hydrothermal [18] method, have shown a higher conversion efficiency compared to those based on disorderedly nanostructure films. However, there is less study on electrodeposited ZnO nanorod arrays based DSSCs. In addition, since the dyes used for DSSCs with a higher efficiency are almost suited for TiO_2, a suitable condition has to be found to sensitize ZnO electrode because of the differences between ZnO and TiO_2. Previous work reveals that the way to sensitize ZnO considerably influenced efficiency [19]. However, fewer researches have been done on investigating the difference in the morphology changes and cell performances by using different dye.

In this paper, electrodeposited ZnO nanorod arrays are used as photoanodes to fabricate DSSCs. The influences of sensitizing conditions and length of nanorods on the cell performances of DSSCs based on ZnO nanorod arrays have been further studied and discussed.

EXPERIMENTAL

1. Synthesis of ZnO Nanorod Arrays

ZnO nanorod arrays were fabricated by one-step cathodic electrochemical deposition from an aqueous solution of zinc nitrate, as described in our previous paper [20]. A Zn foil (99.99% purity) and an ITO-coated glass substrate (pretreated by sonication in absolute ethanol and de-ionized water successively then dried in air at 40 °C) were used as the counter electrode and the working electrode, respectively. The electrodeposition occurred in a glass cell at a constant temperature of 70 °C immersed in a water bath. The initial pH value was about 6, with the electrolyte of an aqueous solution containing 5 mM $Zn(NO_3)_2$. The deposition current was fixed at 0.9 mA. After certain time from 2 h to 8 h of electrodeposition, ZnO nanorod arrays were obtained. Subsequently, the products were rinsed with distilled water several times and dried at room temperature. The surface morphology of the as-deposited ZNR arrays was characterized by a field-emission scanning electron microscope (FE-SEM, Hitachi S-4800FEG). The crystal structure and phase identification were examined by X-ray diffraction (XRD, Philips X'Pert with Cu Kα radiation).

2. Dye Adsorption and Cell Fabrication

The ZNR arrays photoelectrode was then immersed in a 0.25 mM ethanol solution of dye N719 or N3 for different time. When loaded with dye molecules, the electrode was washed with ethanol and dried in air. An electrodeposited platinum conductive glass was used

†To whom correspondence should be addressed.
E-mail: linyuyrr@163.com

as the counter electrode. The two electrodes were clipped together and one drop of liquid electrolyte was kept between them. Finally, a piece of cyano acrylate adhesive (30 mm) was used as a sealant. Bisphenol A epoxy resin was used for the further sealing process. The liquid electrolyte contained 0.4 M sodium iodide, 0.1 M tetrabutyl ammonium iodide, 0.5M4-tert-butylpyridine and 0.05Miodine in an acetonitrile solution.

3. Photo-electrochemical Measurements

Photo-electrochemical tests were made by measuring the J-V characteristic curves under simulated AM 1.5 solar illumination at 100 mW cm^{-2} from a xenon arc lamp (CHF-XM500, Trusttech Co., Ltd., China) in an ambient atmosphere and recorded using a CHI 660 C electrochemical workstation (CH Instrument Inc., China).

RESULTS AND DISCUSSION

1. Influence of Dye Etching on the Morphology of ZnO Nanorods

Fig. 1 displays the typical plan-view and cross-sectional SEM images of the ZnO nanorods arrays electrodeposited on ITO-coated glass substrate from 5 mM $Zn(NO_3)_2$ aqueous solution at 70 °C and 0.9 mA when the deposition duration was 4 h. The whole surface of substrate is uniformly covered by dense hexagonal ZnO nanorods with planar ends which c-axes are perpendicular to the substrate and mainly 450 nm in diameter and 4.1 μm in length approximately. With different duration of deposition, the length can be controlled from 2 μm to 10 μm [20].

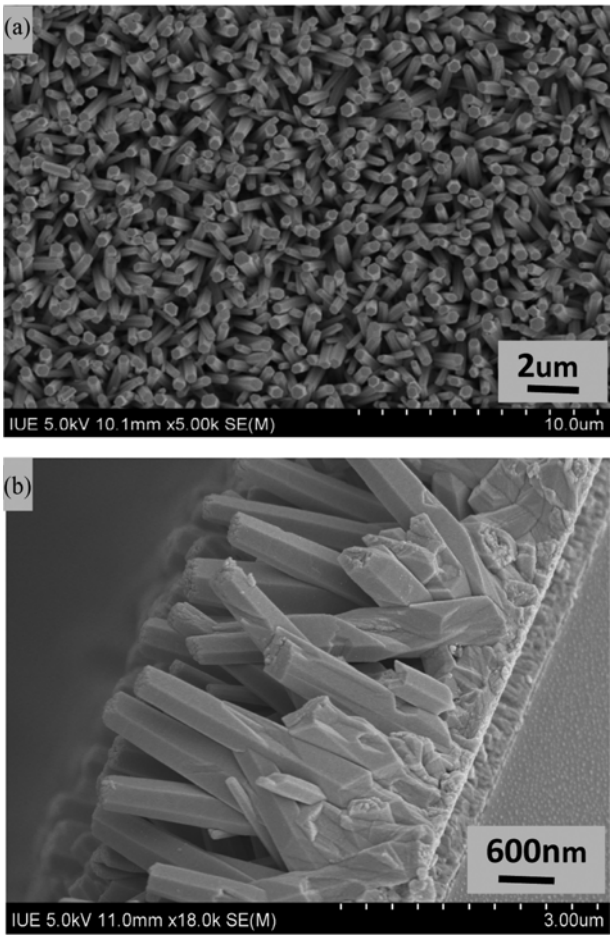

Fig. 1. Typical plan-view (a) and cross-sectional (b) FE-SEM micrographs of electrodeposited ZnO nanorod arrays from a 5 mM $Zn(NO_3)_2$ aqueous solution at 70 °C and 0.9 mA for 4 h.

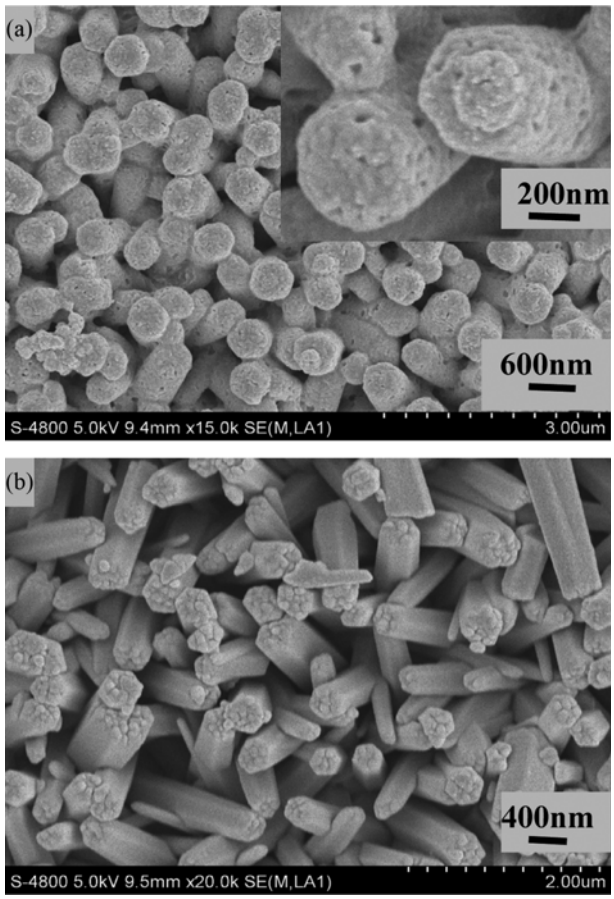

Fig. 2. SEM images of (a) ZnO nanorod arrays sensitized with N719 for 24 h; (b) ZnO nanorod arrays sensitized with N3 for 24 h.

Fig. 2 presents SEM images of the ZnO nanorod electrode after sensitizing with N719 and N3 for 24 h, respectively. After being sensitized for certain time, the surfaces of nanorods are etched by both dyes. It has been reported that this surface structure destruction may due to the formation of Zn^{2+}/dye complex, which always occurs when the electrode is soaked in the dye solution for a time [21]. Apparently, N719 have a larger damage to the structure. The hexagonal nanorods are dissolved to cylinder with many etch pits on the surfaces. In comparison, N3 is less harmful to ZnO which only destroyed the top of nanorods in the same duration of sensitizing. To sum up, dyes etch ZnO electrode and continue over time when the sample is immersed into the dye solution. Therefore, the time of sensitizing is not the longer the better. It is important to find a proper condition of sensitizing to lessen etching.

Both N3 and N719 have -COOH groups which are easy to make the solution acidic by hydrolyzed hydrogen ions. The acidic dye solution is harmful to the amphoteric oxide ZnO. Moreover, the previous paper reported that the formation of aggregates (dye/Zn^{2+}) of dyes with Zn^{2+} ions results in inefficient electron injection from the dye/Zn^{2+} aggregates to the ZnO photoanodes [22]. The etching of ZnO nanorods can be described as the following chemical reaction:

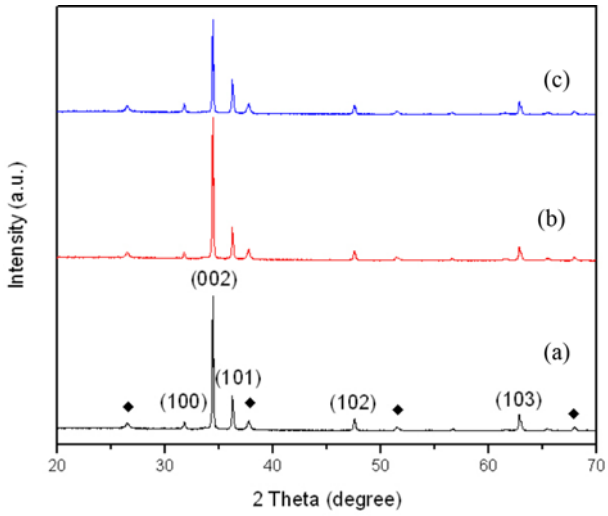

Fig. 3. XRD patterns of (a) ZnO nanorod arrays; (b) ZnO nanorod arrays sensitized with N3; (c) ZnO nanorod arrays sensitized with N719. The peaks marked ◆ represent the ITO substrate.

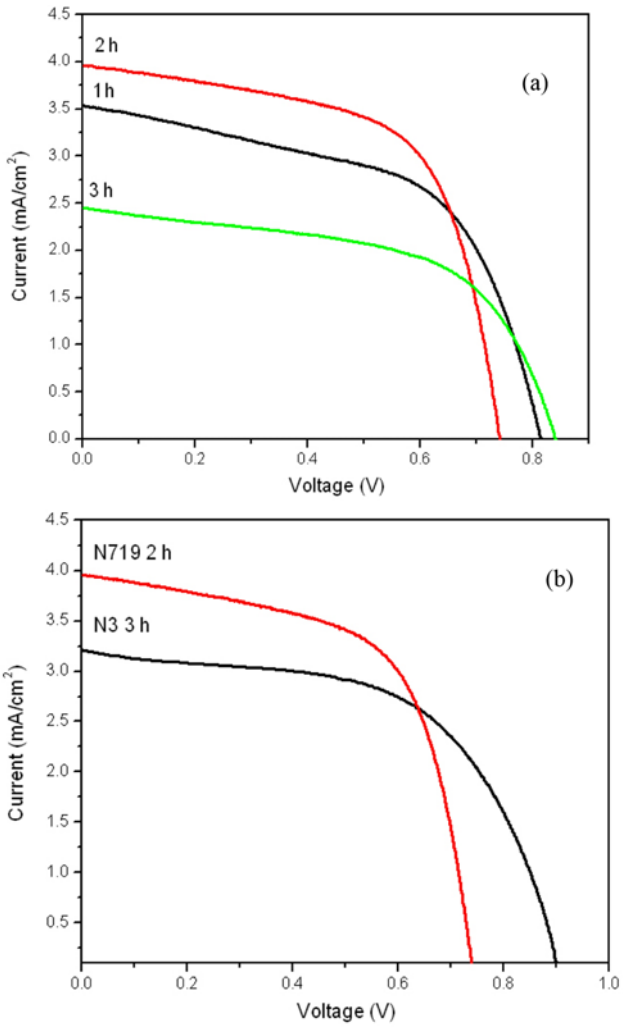

Fig. 4. J-V curves of DSSCs based on ZnO nanorod arrays electrode (a) sensitized with N719 for 1 h, 2 h, and 3 h; (b) sensitized with N3 for 3 h and N719 for 2 h.

$ZnO+H^+ \rightarrow ZnOH$

$ZnOH \rightarrow Zn^{2+}+OH^-$

$Zn^{2+}+dyes \rightarrow aggregates\ (dye/Zn^{2+})$

H^+ is adsorbed to the ZnO surface and produces hydroxyl groups. On the other hand, Zn^{2+} is easily combined with the -COOH groups of dyes under acidic conditions, which accelerates the etching of ZnO. N719 is the bideprotonated form of N3. The COO- groups with negative charge of N719 in solution more easily catch Zn^{2+} and form aggregates (dye/Zn^{2+}). So N719 is more harmful to ZnO structures.

From the XRD patterns of Fig. 3, all the samples are characterized as wurtzite structure of ZnO. Sharp diffraction peaks indicate good crystallinity, and the strongest diffraction peak corresponding to the plane (0 0 2) reveals preferential crystal growth along the c-axis in the [0001] direction vertical to the substrates. The other peaks of ZnO may be caused by the imperfection of vertical alignment. The left major peaks were all from the ITO substrate. Although etched with dyes, there is no obvious change with the crystallinity of ZnO except for a decrease in peak intensity. This loss is likely due to the lower crystalline quality of ZNR after a long etching time. Besides, no new phase and impurities diffraction peaks like $Zn(OH)_2$ and Zn were detected. In addition, XRD can be used as an auxiliary method to prove the verticality of the obtained ZnO nanorod arrays.

2. Influence of Dye Etching on the Cell Performance

Fig. 4(a) shows the J-V curves for ZNR electrode sensitized with N719 for different time. The detailed parameters can be seen from Table 1. The performance of cells reached the top efficiency η=1.82% when the sensitizing time was 2 h, and began to decrease quickly with the sensitizing time increasing. The results can be explained by surface etching, which damaged the outer structure of ZnO nanorod according to the SEM pictures. The sharp decrease of short-circuit density (Jsc) from 3.53 mA/cm^2 to 1.43 mA/cm^2 is largely due to the formation of aggregates (dye/Zn^{2+}) and the surface etching.

In comparison, N3 dye etching has little influence on the perfor-

Table 1. Parameters of DSSCs based on ZnO nanorod array with different dyes and sensitizing time

Dyes/Sensitizing time	Voc (V)	Jsc (mA/cm^2)	FF	η (%)
N719/1 h	0.814	3.53	0.56	1.61
N719/2 h	0.741	3.95	0.62	1.81
N719/3 h	0.841	2.45	0.56	1.17
N719/24 h	0.496	1.43	0.36	0.26
N3/1 h	0.822	2.90	0.56	1.34
N3/2 h	0.826	3.29	0.60	1.63
N3/3 h	0.900	3.21	0.58	1.68
N3/4 h	0.850	2.90	0.59	1.54
N3/24 h	0.801	1.03	0.49	0.41

Table 2. Parameters of DSSCs based on ZnO nanorod with different electrodeposition time

Electrodeposition time	Voc (V)	Jsc (mA/cm^2)	FF	η (%)
2 h	0.731	3.14	0.62	1.43
4 h	0.741	3.95	0.62	1.81
8 h	0.765	4.95	0.64	2.46

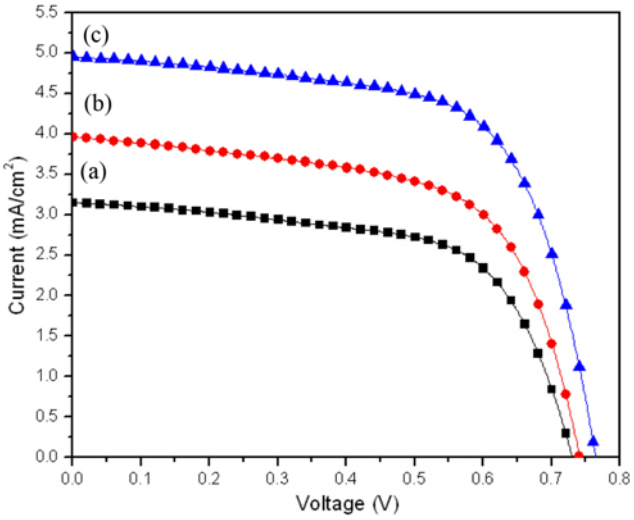

Fig. 5. J-V curves of DSSCs based on ZnO nanorod with different electrochemical deposition time: (a) 2 h; (b) 4 h; (c) 8 h.

mance of cells, as shown in Table 2. With longer sensitizing time, the efficiency did not drop quickly and the top efficiency was also slightly lower than N719 cells, as shown in Fig. 4(b). It is reported that the absorption spectra of the samples coated with the N719 dye were broader than that coated with the N3 dye [23]. It explains that the DSSC with N719 dye has a better photovoltaic performance than the DSSC with the N3 dye.

3. Influence of Electrodeposition Time on the Cell Performance

As reported in our previous paper, various deposition times can change the length of ZnO nanorods, ranging from 2 μm to 10 μm [20]. Fig. 5 and Table 2 show the performance of cells when electrodeposition times are 2 h, 4 h and 8 h, respectively. Through the experiments above, we chose N719 dye and 2 h sensitizing time as the best sensitizing condition. From Fig. 5 and Table 2, the efficiency exhibits a continuous increase with electrodeposition times. The photocurrent Jsc and open circuit potential Voc increased from 3.14 mA/cm^2 and 0.73 V to 4.9 mA/cm^2 and 0.77 V, respectively. Conversion efficiency can be as high as η=2.46%, which is higher than that of DSSCs based on ZNR photoanode fabricated by CVD (1.82%) and hydrothermal method (2.4%). The increase of DSSC efficiency as a function of electrodeposition time probably is associated with the enhanced surface area and higher surface concentration of dye. It is entirely possible that the performance of ZnO nanorod based DSSC would be better with a longer ZnO nanorod electrode in a certain range.

CONCLUSIONS

In summary, the surfaces of ZnO nanorods were etched by dye solutions, no matter whether N3 or N719. So the performance of cells was influenced by different sensitizing time. Compared with N3, the N719 have greater damage to the structure of ZNR photoanodes, and the performance of cells decreased quickly with the sensitizing time increasing. In a certain range, the cell efficiency exhibits a continuous increase with electrodeposition times.

ACKNOWLEDGEMENTS

This work was supported by the Fundamental Research Funds for the Central Universities (Grant No. JB - ZR1137).

REFERENCES

1. M. Gratzel, *J. Photochem. Photobiol. C*, **4**, 145 (2003).
2. A. Yella, H. W. Lee, H. N. Tsao, C. Y. Yi, A. K. Handiran, M. K. Nazeeruddin, E. W. Diau, C. Y. Yeh, S. M. Zakeeruddin and M. Gratzel, *Science*, **334**, 629 (2011).
3. J. H. Wu, S. C. Hao, Z. Lan, J. M. Lin, M. L. Huang, Y. F. Huang, P. J. Li, S. Yin and T. Sato, *J. Am. Chem. Soc*., **130**, 11568 (2008).
4. Z. Lan, J. H. Wu, S. C. Hao, J. M. Lin, M. L. Huang and Y. F. Huang, *Energy Environ. Sci*., **2**, 524 (2009).
5. J. Ya, L. An, Z. Liu, L. E, W. Zhao, D. Zhao and C. Liu, *Korean J. Chem. Eng*., **29**, 731 (2012).
6. Q. Zhang, C. S. Dandeneau, X. Zhou and G. Z. Cao, *Adv. Mater*., **21**, 4087 (2009).
7. T. Yoshida, H. Minoura, J. Zhang, D. Komatsu, S. Sawatani, T. Pauporte, D. Lincot, T. Oekermann, D. Schlettwein, H. Tada, D. Wohrle, K. Funabiki, M. Matsui, H. Miura and H. Yanagi, *Adv. Funct. Mater*., **19**, 17 (2009).
8. H. M. Cheng and W. F. Hsieh, *Energy Environ. Sci.*, **3**, 442 (2010).
9. F. Xu and L. T. Sun, *Energy Environ. Sci.*, **4**, 818 (2011).
10. Y. B. Hahn, *Korean J. Chem. Eng*., **28**, 1797 (2011).
11. A. Petersson, M. Ratner and H. O. Karlsson, *J. Phys. Chem. B*, **104**, 8498 (2000).
12. C. Bauer, G. Boschloo, E. Mukhtar and A. Hagfeldt, *J. Phys. Chem. B*, **105**, 5585 (2001).
13. L. M. Peter, *J. Phys. Chem. Lett*., **2**, 1861 (2011).
14. M. Law, L. E. Greene, J. C. Johnson, R. Saykally and P. Yang, *Nat. Mater*., **4**, 455 (2005).
15. E. Hosono, S. Fujihara, I. Honma and H. Zhou, *Adv. Mater*., **17**, 2091 (2005).
16. R. S. Mane, W. J. Lee, H. M. Pathan and S. H. Han, *J. Phys. Chem. B*, **109**, 24254 (2005).
17. M. H. Lai, M. W. Lee, G. J. Wang and M. F. Tai, *Int. J. Electrochem. Sci*., **6**, 2122 (2011).
18. M. Guo, P. Diao, X. D. Wang and S. M. Cai, *J. Solid State Chem.*, **178**, 3210 (2005).
19. F. P. Yan, L. H. Huang, J. S. Zheng, J. Huang, Z. Lin, F. Huang and M. D. Wei, *Langmuir*, **26**, 7153 (2010).
20. Y. Lin, J. Y. Yang and X. Y. Zhou, *Appl. Surf. Sci*., **258**, 1491 (2011).
21. K. Keis, C. Bauer, G. Boschloo, A. Hagfeldt, K. Westermark, H. Rensmo and H. Siegbahn, *J. Photochem. Photobiol. A*, **148**, 57 (2002).
22. J. J. Wu, G. R. Chen, H. H. Yang, C. H. Ku and J. Y. Lai, *Appl. Phys. Lett*., **90**, 213109 (2007).
23. M. Y. A. Rahman, A. A. Umar, R. Taslim and M. M. Salleh, *Electrochim. Acta*, **88**, 639 (2013).